HDAC7 is an immunometabolic switch triaging danger signals for engagement of antimicrobial versus inflammatory responses in macrophages

Kaustav das Gupta, Divya Ramnath, Jessica von Pein, James Curson, Yizhuo Wang, Rishika Abrol, Asha Kakkanat, Shayli Varasteh Moradi, Kimberley Gunther, Ambika Murthy, et al.

PNAS RESEARCH ARTICLE | MICROBIOLOGY

HDAC7 is an immunometabolic switch triaging danger signals for engagement of antimicrobial versus inflammatory responses in macrophages

Kaustav Das Gupta[a], Divya Ramnath[a], Jessica B. von Pein[a], James E. B. Curson[a], Yizhuo Wang[a], Rishika Abrol[a], Asha Kakkanat[b], Shayli Varasteh Moradi[c], Kimberley S. Gunther[a], Ambika M. V. Murthy[a], Claudia J. Stocks[a], Ronan Kapetanovic[a], Robert C. Reid[a], Abishek Iyer[a], Zoe C. Ilka[a], William M. Nauseef[d], Manuel Plan[e], Lin Luo[a], Jennifer L. Stow[a], Kate Schroder[a], Denuja Karunakaran[a], Kirill Alexandrov[c], Melanie R. Shakespear[a], Mark A. Schembri[b], David P. Fairlie[a], and Matthew J. Sweet[a,1]

Edited by Katherine Fitzgerald, University of Massachusetts Medical School, Worcester, MA; received August 8, 2022; accepted November 21, 2022

The immune system must be able to respond to a myriad of different threats, each requiring a distinct type of response. Here, we demonstrate that the cytoplasmic lysine deacetylase HDAC7 in macrophages is a metabolic switch that triages danger signals to enable the most appropriate immune response. Lipopolysaccharide (LPS) and soluble signals indicating distal or far-away danger trigger HDAC7-dependent glycolysis and proinflammatory IL-1β production. In contrast, HDAC7 initiates the pentose phosphate pathway (PPP) for NADPH and reactive oxygen species (ROS) production in response to the more proximal threat of nearby bacteria, as exemplified by studies on uropathogenic *Escherichia coli* (UPEC). HDAC7-mediated PPP engagement via 6-phosphogluconate dehydrogenase (6PGD) generates NADPH for antimicrobial ROS production, as well as D-ribulose-5-phosphate (RL5P) that both synergizes with ROS for UPEC killing and suppresses selective inflammatory responses. This dual functionality of the HDAC7-6PGD-RL5P axis prioritizes responses to proximal threats. Our findings thus reveal that the PPP metabolite RL5P has both antimicrobial and immunomodulatory activities and that engagement of enzymes in catabolic versus anabolic metabolic pathways triages responses to different types of danger for generation of inflammatory versus antimicrobial responses, respectively.

uropathogenic *Escherichia coli* | macrophages | immunometabolism | inflammation | pentose phosphate pathway

Significance

Macrophages are innate immune cells that use pattern recognition receptors such as the toll-like receptors (TLRs) to sense danger. Individual TLRs detect danger in different contexts, for example, microbial products on the surface of bacteria indicative of nearby or proximal threats, as well as soluble factors representing far away or distal threats. Through studies on uropathogenic *E. coli*, we identify a macrophage pathway that discriminates between proximal and distal danger to engage antimicrobial or inflammatory responses, respectively. The significance of this study lies in the identification of antiinflammatory and antimicrobial activities of the metabolite D-ribulose-5-phosphate, as well as avenues for selectively manipulating host defense versus inflammation. Our findings can be exploited for the design of host-directed therapies and/or antiinflammatory agents.

All organisms must defend themselves against infection or injury to maintain host integrity. In vertebrates, innate immune cells such as macrophages need to detect and respond to both proximal dangers such as nearby pathogens that require destruction, as well as far or distal dangers that are associated with soluble factors and that require immune cell recruitment. Macrophages must be able to prioritize responses to such distinct threats. One mechanism of triage involves engaging different pattern recognition receptors (PRRs), enabling cells to interpret the type of danger and respond accordingly (1). For example, both transmembranal toll-like receptor 4 (TLR4) (2) and cytosolic inflammatory caspases (3, 4) detect Gram-negative bacterial lipopolysaccharide (LPS). Individual danger signals can also be sensed by a single PRR in different contexts. TLR4, for example, detects both soluble LPS and LPS on Gram-negative bacterial surfaces. The former requires initiation of inflammation for leukocyte recruitment, while the latter requires engagement of antimicrobial responses for pathogen destruction. How such context-dependent recognition generates distinct biological outcomes is unknown. In this study, we used the globally significant bacterial pathogen uropathogenic *Escherichia coli* (UPEC), which causes approximately 80% of all urinary tract infections and is a common cause of sepsis (5), to investigate molecular mechanisms of context-dependent immune recognition.

Metabolic pathways influence how innate immune cells respond to danger. TLR signaling activates proinflammatory transcription factors (6) for inducible gene expression (1). TLR signaling also increases glycolysis in macrophages (7), with this required for inflammatory gene expression. This partly reflects the need for an acetyl-CoA pool required for histone acetylation (8). Mechanistically, the glycolytic enzyme pyruvate kinase M2 (PKM2) links glycolysis and inflammation. PKM2 catalyzes the last rate-limiting step in glycolysis and also has a moonlighting inflammatory function via interactions with the transcription factors HIF-1α (9, 10) and STAT3 (9). TLR-inducible glycolysis drives the expression of both the neutrophil-recruiting cytokine IL-1β (10) and the monocyte-recruiting chemokine CCL2 (11), implicating this metabolic response in leukocyte recruitment and inflammation. Metabolic reprogramming has mainly been investigated in the context of soluble danger signals, such as individual TLR ligands.

The authors declare no competing interest.

This article is a PNAS Direct Submission.

[1]To whom correspondence may be addressed. Email: m.sweet@imb.uq.edu.au.

This article contains supporting information online at https://www.pnas.org/lookup/suppl/doi:10.1073/pnas.2212813120/-/DCSupplemental.

Published January 17, 2023.

During infection, innate immune cells typically encounter danger signals that present as particulate matter. Microbial phagocytosis by macrophages and neutrophils is coupled to the rapid generation of reactive oxygen species (ROS) (12, 13), a response mediated by the multimeric NADPH oxidase that assembles on phagosomal membranes (14). Genetic defects in NADPH oxidase components, such as *CYBB* that encodes NOX2, result in chronic granulomatous disease (CGD). CGD patients incur recurrent and life-threatening infections (15). In addition to its antimicrobial role, the phagocyte NADPH oxidase also limits inflammasome activation and secretion of mature IL-1β (16–18). There may be important clinical manifestations of this pathway since CGD patients are susceptible to a range of inflammatory conditions (19, 20). The pentose phosphate pathway (PPP) generates NADPH to fuel phagocyte oxidase-dependent oxidant production (21, 22), but how this pathway integrates innate immune responses to different types of danger is not well understood.

Regulated lysine acetylation on target proteins (23) controls cell metabolism (7, 24). Of the 18 histone deacetylase (HDAC) enzymes (HDAC1-11, SIRT1-7), many have key roles in immune cell development and function (25). Class IIa HDACs (HDAC 4, 5, 7, 9) have multifaceted cellular functions. They can act as transcriptional derepressors for inducible gene expression upon nuclear-cytoplasmic shuttling, transcriptional activators through cytoplasmic to nuclear translocation, and scaffolds or modifiers of non-nuclear substrates (26, 27). These enzymes regulate glucose metabolism (28) and one family member, HDAC7, promotes both glycolysis and glycolysis-associated inflammatory mediators (IL-1β and CCL2) in macrophages responding to soluble LPS (11, 29). We considered that immunometabolic processes may influence how innate immune cells interpret proximal versus distal threats. Given its role in metabolic and inflammatory responses, HDAC7 was of particular interest. Here, we report that HDAC7 is a cytoplasmic metabolic switch in macrophages. In contrast to the glycolysis-linked proinflammatory signal delivered by HDAC7 in macrophages responding to distal danger, we show that this lysine deacetylase engages the PPP in response to proximal danger. Its activation of the PPP enzyme 6-phosphogluconate dehydrogenase (6PGD) generates NADPH for antimicrobial ROS, as well as D-ribulose-5-phosphate (RL5P) that serves dual roles in contributing to ROS-dependent UPEC killing and suppressing specific inflammatory responses. Our findings reveal a molecular mechanism by which macrophages recognize the context of danger signals to shape appropriate immune responses, and also identify antimicrobial and immunomodulatory functions of RL5P.

Results

HDAC7 Discriminates between Distal and Proximal Threats during Macrophage Activation. To interrogate our model that immunometabolism controls context-dependent danger recognition (Fig. 1*A*), we employed soluble TLR agonists as surrogates of distal danger and either live bacteria or TLR agonists plus particles as mimics of proximal danger. To perturb macrophage metabolism, we antagonized HDAC7 function (11) and monitored IL-1β production as a read-out of glycolysis-associated inflammatory responses (10). Remarkably, HDAC7 inhibition with the class IIa HDAC inhibitor TMP195 (30) suppressed inflammasome-triggered IL-1β release from primary human macrophages primed with soluble LPS, whereas this response was significantly enhanced in HMDM responding to UPEC strain EC958 (Fig. 1*B*). The IL-1β response was also enhanced in macrophages responding to the combination of LPS plus latex beads as a mimic of proximal danger (Fig. 1*B*), confirming that the effect of UPEC was not due to pathogen subversion of macrophage functions. Glycolysis also promotes TNF production in human macrophages (31) and here we found that HDAC7 inhibition similarly reprogrammed the inducible TNF response in macrophages responding to stimuli indicative of either distal or proximal danger (Fig. 1*C*), albeit the consistent and pronounced inhibitory effect of TMP195 on LPS-induced TNF was not statistically significant for the sample size. These data suggest that HDAC7 has opposing roles in controlling inflammatory responses in human macrophages responding to distal versus proximal danger.

In primary mouse bone marrow-derived macrophages (BMM), the opposing effect of LPS versus UPEC on IL-1β release was apparent after genetic (Fig. 1 *D* and *E*) or pharmacological (*SI Appendix*, Fig. S1*A*) targeting of HDAC7. IL-1β release requires both TLR-inducible expression of pro-IL1β, as well as inflammasome-mediated processing for IL-1β maturation (32). Since both pro-IL-1β production (cell lysates) and processed IL-1β secretion (culture supernatants) were differentially affected by distal (LPS) versus proximal (EC958) danger signals (Fig. 1*D*), we conclude that HDAC7 exerts its effects through TLR signaling, rather than inflammasome activation. Consistent with this, HDAC7 did not affect inflammasome-triggered BMM cell death, irrespective of the priming signal (*SI Appendix*, Fig. S1*B*). In contrast to our observations in HDAC7-inhibited HMDM (Fig. 1*C*), *Hdac7* deletion did not affect LPS- or *Escherichia coli*-inducible TNF release (*SI Appendix*, Fig. S1*C*). However, pharmacological inhibition of HDAC7 in BMM did reduce LPS-induced TNF, without affecting the response to UPEC (*SI Appendix*, Fig. S1*D*). The reduction in LPS-induced TNF by HDAC7 inhibition in HMDM (Fig. 1*C*) and BMM (*SI Appendix*, Fig. S1*D*) may reflect targeting of multiple class IIa HDACs (11), given that *Hdac7* deletion had no effect on this response (*SI Appendix*, Fig. S1*C*). However, this does not explain the distinct effects of HDAC7 inhibition on TNF responses in human versus mouse macrophages responding to UPEC (Fig. 1*C* and *SI Appendix*, Fig. S1*D*), with species-specific regulation of TLR responses potentially contributing to these differences (33). Analysis of gene expression confirmed the selective role of HDAC7 in differentially regulating IL-1β in macrophages responding to distal versus proximal danger signals. In *Hdac7*-deficient BMM, LPS- and UPEC-induced *Il1b* mRNA levels were attenuated and amplified, respectively (*SI Appendix*, Fig. S1*E*). In contrast, inducible expressions of *Tnf, Il6*, and *Cxcl12* were unaffected in the same samples (*SI Appendix*, Fig. S1 *F–H*). Moreover, pharmacological inhibition of HDAC7 did not affect LPS- or UPEC-induced IL-6 secretion in BMM (*SI Appendix*, Fig. S1*I*). These findings point to differential and selective control of pro-IL-1β production by HDAC7 in macrophages responding to distal versus proximal danger.

Next, we expanded our repertoire of surrogates of proximal versus distal danger and controls to further interrogate our model. Here, we found that the increase in UPEC-induced IL-1β upon *Hdac7* deletion was apparent over a multiplicity of infection (MOI) range (*SI Appendix*, Fig. S2*A*) and that HDAC7 differentially affected the production of IL-1β (Fig. 1*F*) but not TNF (*SI Appendix*, Fig. S2*B*) in BMM responding to LPS versus LPS-coated latex beads. Importantly, inducible IL-1β production was strictly TLR4-dependent in BMM responding to mimics of either distal danger (LPS) or proximal danger (LPS plus beads) (*SI Appendix*, Fig. S2*C*). Distinct effects of HDAC7 on IL-1β (*SI Appendix*, Fig. S2*D*) but not TNF (*SI Appendix*, Fig. S2*E*) were also apparent when comparing the TLR2 agonist Pam3CSK4 versus Pam3CSK4 plus latex beads, thus confirming the generality of the phenomenon. Thus, HDAC7 promotes or inhibits IL-1β in both human and mouse macrophages responding to signals of distal versus proximal danger, respectively.

Production of pro-IL-1β is controlled by glucose metabolism (10, 34). We previously demonstrated that HDAC7 instructs LPS-inducible glycolysis in macrophages (11, 29), so we next focused

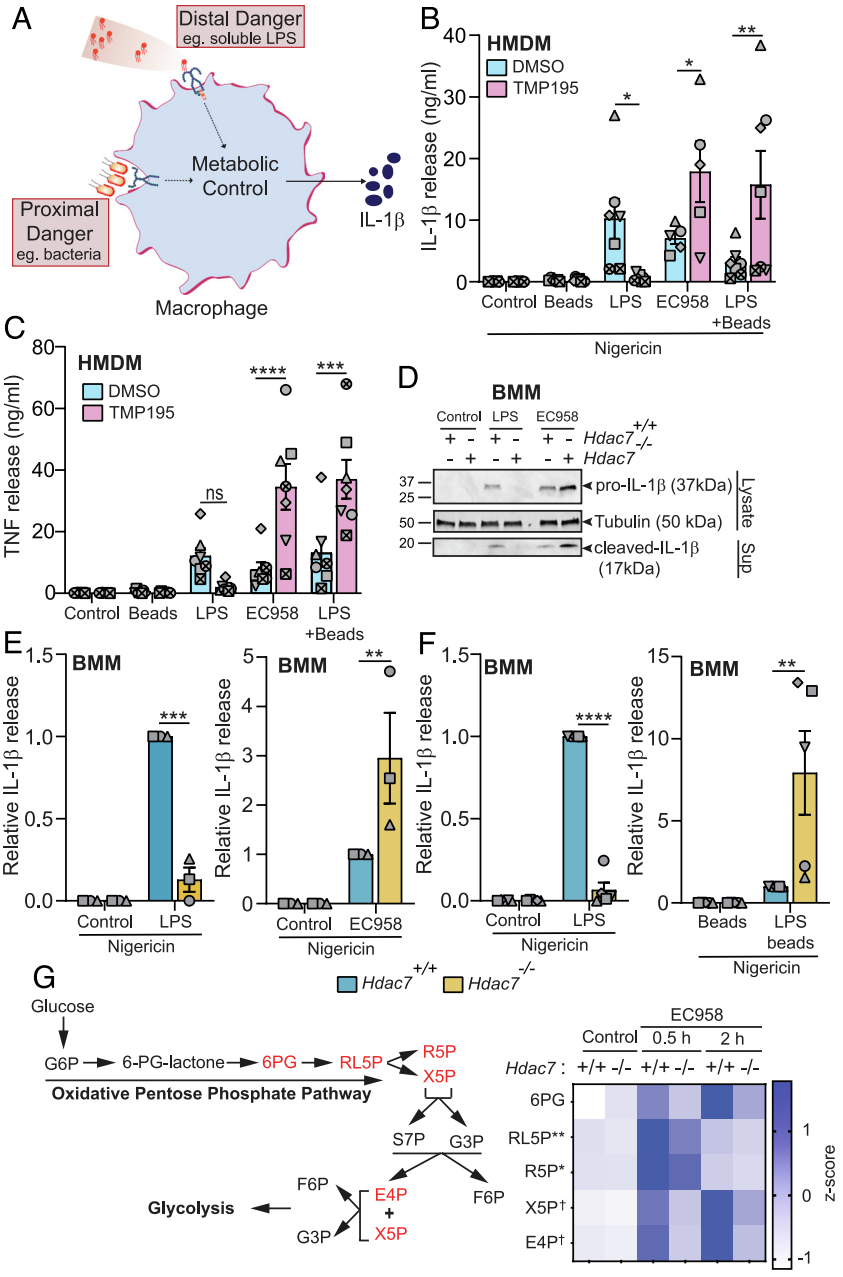

Fig. 1. HDAC7 discriminates between distal and proximal threats during macrophage activation. (*A*) Model of immunometabolic control of macrophage responses to distal versus proximal danger signals. (*B* and *C*) IL-1β and TNF release from HMDM pretreated with TMP195 (10 μM) for 1 h followed by LPS (100 ng/mL), EC958 (MOI 100), or LPS and latex beads for 4 h. Additional nigericin (5 μg/mL) treatment for 2 h followed, where indicated. (*D*) Immunoblots for pro- and cleaved-IL-1β in indicated BMM populations treated with either LPS (1 ng/mL) or infected with EC958 (MOI 10) for 4 h, followed by nigericin for 1 h (representative of four independent experiments). (*E* and *F*) IL-1β release from the indicated BMM populations treated with either LPS (0.5 ng/mL; *Left*, *E* and *F*), infected with EC958 (MOI 10; *E*, *Right*), or LPS-coated latex beads (*F*, *Right*) for 4 h, followed by nigericin for 1 h. (*G*) A heatmap showing the expression patterns of pentose phosphate pathway metabolites (highlighted in red) in lysates from wild-type ($Hdac7^{+/+}$) and $Hdac7^{-/-}$ BMM infected with EC958 (MOI 100, 30 min and 2 h). * and ** indicate statistical comparison between $Hdac7^{+/+}$ and $Hdac7^{-/-}$ BMM at 30 min postinfection, and † indicates statistical comparison between $Hdac7^{+/+}$ and $Hdac7^{-/-}$ BMM at 2 h postinfection. Graphical data (mean ± SEM, n = 3 to 7) are combined from three to seven independent experiments (or donors) performed in experimental duplicate. Data are normalized to the $Hdac7^{+/+}$ LPS-treated, EC958-infected, or LPS-coated latex beads (*E* and *F*). Statistical significance was determined using repeated measure two-way ANOVA followed by Sidak's multiple comparison test (ns, not significant; $*P < 0.05$; $**P < 0.01$; $***P < 0.001$; $****P < 0.0001$; $†P < 0.05$).

on understanding the role of HDAC7 in regulating metabolic responses in macrophages responding to proximal danger. To do so, we compared central carbon metabolites in wild-type versus *Hdac7*-deficient macrophages infected with UPEC. Challenge with UPEC resulted in increased levels of both PPP and glycolytic metabolites (Fig 1*G* and *SI Appendix*, Fig. S2*F* and Table S1). *Hdac7* deficiency attenuated the inducible production of several PPP intermediates including ribulose-5-phosphate, ribose-5-phosphate, xylulose-5-phosphate, and erythrose-4-phosphate (Fig. 1*G* and *SI Appendix*, Table S1), thus revealing that HDAC7 both promotes the PPP and inhibits specific inflammatory responses in macrophages responding to the proximal threat of nearby bacteria. Collectively, these data support a model in which HDAC7 directs distinct metabolic and inflammatory responses, depending on the context of the stimulus.

HDAC7 Is Required for Macrophage-Mediated *Escherichia coli* Uptake and Clearance. Given its role in directing the PPP in macrophages responding to UPEC, as well as its opposing effects on inflammatory responses in macrophages responding to proximal versus distal danger, we next considered that HDAC7 functions may be redeployed toward antimicrobial defense when nearby threats are encountered. Indeed, HDAC7 was required for rapid clearance of UPEC in BMM, as assessed by both genetic targeting (Fig. 2*A*) and pharmacological inhibition with TMP195 (Fig. 2*B*). A similar phenotype was also observed in human macrophage-like PMA-differentiated THP-1 cells (*SI Appendix*, Fig. S3*A*). TMP195 did not affect *Escherichia coli*-infected BMM or THP-1 viability (*SI Appendix*, Fig. S3 *B* and *C*) or bacterial growth (*SI Appendix*, Fig. S3*D*), thus indicating that the increased bacterial loads in TMP195-treated macrophages were a consequence of impaired host defense. The effect of HDAC7 inhibition was apparent when cells were preincubated with TMP195 prior to infection with *Escherichia coli*, but not when cells were treated 1 h after *Escherichia coli* challenge (Fig. 2*C*). This implies that HDAC7 engages rapid antimicrobial responses in macrophages responding to proximal danger.

Phagocytosis is coupled to the engagement of immediate antimicrobial responses (35). The increased intracellular bacterial loads

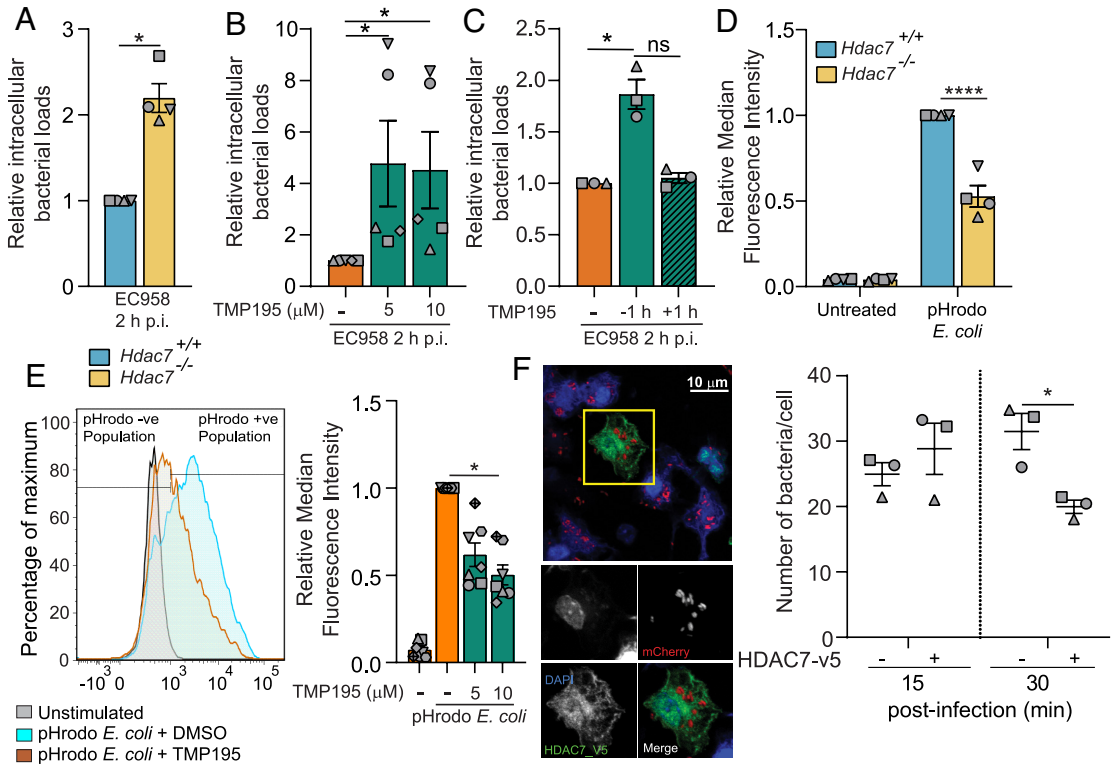

Fig. 2. HDAC7 is required for macrophage-mediated *Escherichia coli* uptake and clearance. (*A*) Relative intramacrophage bacterial loads at 2 h p.i. in BMM infected with UPEC strain EC958. (*B*) Relative intramacrophage loads of EC958 at 2 h p.i. in BMM pretreated with the indicated concentrations of TMP195 for 1 h prior to infection. (*C*) Relative intramacrophage loads of EC958 at 2 h p.i. in BMM either pretreated with TMP195 for 1 h prior to infection or 1 h p.i. (*D*) Phagocytic uptake of pHrodo *Escherichia coli* in indicated BMM populations. (*E*) Phagocytic uptake of pHrodo *Escherichia coli* in BMM pretreated with the indicated concentrations of TMP195 for 30 min prior to treatment with pHrodo *Escherichia coli*. Representative flow cytometry plot for BMM (*Left*) as well as relative median fluorescence intensity (MFI) data (*Right*) are shown. (*F*) Mac-Hdac7 BMM were spin-infected with MG1655_mCherry for 5 min, after which cells were fixed at the indicated time points. Immunofluorescence was performed to detect cells harboring fluorescent bacteria. The indicated image (*Left*) is representative of three independent experiments. Manual quantification of bacterial numbers (*Right*) was performed across multiple images (minimum 26 cells per time point, per experiment) utilizing ImageJ. Graphical data (mean ± SEM, n = 3 to 7) are combined from three to seven independent experiments performed in experimental duplicates and are normalized to the *Hdac7*$^{+/+}$ (*A* and *D*) or the no TMP195 control sample (*B*, *C*, and *E*). Statistical significance was determined using unpaired nonparametric Mann–Whitney test (*A*), Kruskal–Wallis test followed by Dunn's multiple comparison test (*B*, *C*, and *E*) or repeated measure two-way ANOVA (*D* and *F*), followed by Sidak's multiple comparison test or (ns, not significant; *$P < 0.05$; ****$P < 0.0001$).

observed in macrophages after HDAC7 targeting might result from enhanced phagocytosis and/or impaired bacterial killing. To address this, we assessed fluorescently labeled heat-killed *Escherichia coli* (pHrodo *Escherichia coli*) uptake, finding that this was significantly impaired in *Hdac7*$^{-/-}$ versus *Hdac7*$^{+/+}$ BMM (Fig. 2*D*) and in PMA-differentiated THP-1 cells after *HDAC7* silencing (*SI Appendix*, Fig. S4 *A* and *B*). Similarly, class IIa HDAC inhibition impaired phagocytosis (~50%) in both BMM (Fig. 2*E*) and PMA-differentiated THP-1 cells (*SI Appendix*, Fig. S4*C*). Given that HDAC7 is required for optimal bacterial uptake (Fig. 2 *D* and *E* and *SI Appendix*, Fig. S4 *B* and *C*), the contribution of this enzyme to bacterial clearance is likely more pronounced than suggested by intracellular bacterial survival data (Fig. 2 *A* and *B* and *SI Appendix*, Fig. S3*A*). Indeed, when performing acute spin-infections to maximize bacterial uptake (20 min p.i.) and assessing bacterial loads at 2 h p.i. relative to those at uptake, HDAC7-inhibited macrophages were strikingly impaired for *Escherichia coli* killing (*SI Appendix*, Fig. S4*D*).

To further interrogate our model that HDAC7 engages antimicrobial responses upon encountering proximal danger, we used myeloid-specific HDAC7-overexpressing (Mac-Hdac7) mice (11) and RAW 264.7 cells stably overexpressing HDAC7 (36) in gain-of-function approaches. In both cases, HDAC7 overexpression enhanced intracellular *Escherichia coli* clearance (*SI Appendix*, Fig. S4 *E* and *F*) and increased *Escherichia coli* uptake (*SI Appendix*, Fig. S4 *G* and *H*). To further monitor the effect of HDAC7 on phagocytosis versus bacterial killing, we used confocal microscopy to visualize intracellular *Escherichia coli* within BMM expressing HDAC7-V5 or not within the same BMM population. At 15 min p.i., HDAC7-V5-overexpressing macrophages accumulated more intracellular bacteria, but by 30 min p.i. bacterial loads per macrophage were significantly reduced (Fig. 2*F*). Collectively, these data establish a key role for HDAC7 in host defense, in addition to its function in suppressing IL-1β production in macrophages responding to proximal danger.

HDAC7 Is Required for Host Defence In Vivo. HDAC7 has a proinflammatory function in vitro and in vivo in response to soluble LPS (11), so we next examined whether myeloid HDAC7 switches to an antimicrobial and antiinflammatory role in mice responding to bacterial infection. C57Bl/6 mice were administered with TMP195 or vehicle control and then infected (i.p.) with UPEC (Fig. 3*A*). Consistent with the heightened IL-1β response observed in vitro (Fig. 1*B* and *SI Appendix*, Fig. S1*A*), TMP195 exacerbated infection-induced hypothermia (Fig. 3*B*), a physiological response mediated by systemic inflammation (37). At 8 h p.i., UPEC loads in peritoneal exudates, the liver and spleen were also substantially increased in TMP195-treated mice (Fig. 3 *C*–*E*). Similar effects on infection-induced hypothermia (Fig. 3*F*) and UPEC burdens (Fig. 3 *G*–*I*) were apparent in myeloid-deficient *Hdac7* knockout mice. End-point analysis of serum cytokines confirmed that UPEC-challenged *Hdac7*-deficient mice displayed significantly elevated levels of the inflammatory mediators TNF and CCL2, with a trend for increased levels of IFNγ and IL-6 (*SI Appendix*, Table S2). The differences in the specific inflammatory signature observed in these in vivo studies by comparison to the in vitro studies in

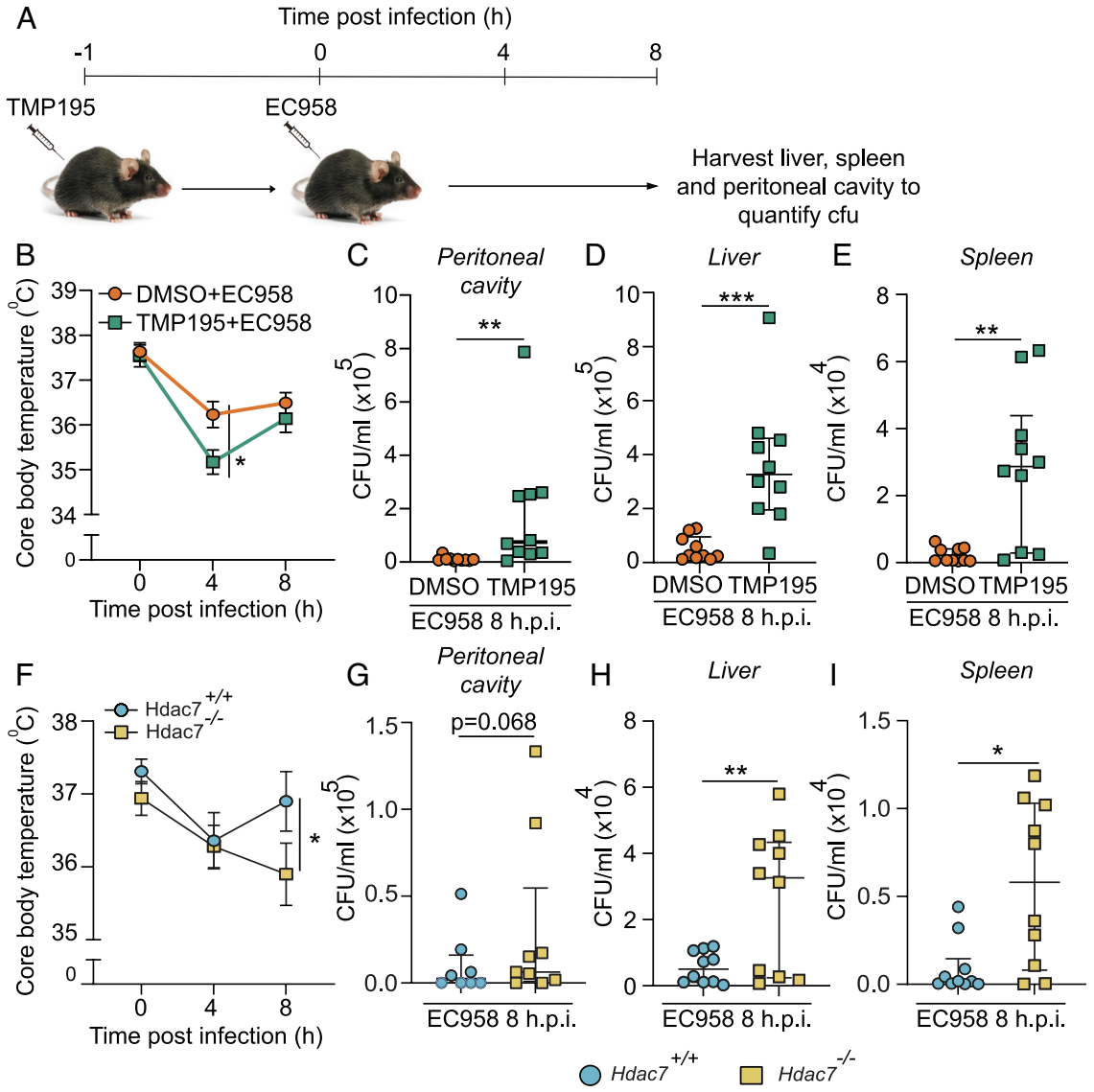

Fig. 3. HDAC7 is required for host defense in vivo. (*A*) Schematic representation of infection strategy. (*B–E*) Core body temperature (*B*) and cfu in peritoneal cavity (*C*), liver (*D*), and spleen (*E*) of C57BL/6J mice infected with EC958 in the presence or absence of TMP195. (*F–I*) Core body temperature (*F*) and cfu in peritoneal cavity (*G*), liver (*H*) and spleen (*I*) of *Hdac7*$^{+/+}$ and *Hdac7*$^{-/-}$ mice infected with EC958. Data show median ± interquartile range of 10 mice per treatment group. Statistical significance was determined by two-way ANOVA (*B* and *F*) or unpaired nonparametric Mann–Whitney test (*C–E* and *G–I*) (*$P < 0.05$; **$P < 0.01$; ***$P < 0.001$).

BMM (Fig. 1 and *SI Appendix*, Fig. S1) likely reflect the time of sampling and the complex nature of the cytokine network in vivo. Collectively, these data confirm that, in response to the proximal threat of a bacterial infection, myeloid HDAC7 both initiates rapid antimicrobial responses for effective host defense and limits inflammatory responses.

Antimicrobial Effects of HDAC7 Require Its Enzymatic Activity and Are Independent of Glycolysis-PKM2. We next addressed the mechanisms by which HDAC7 switches from its proinflammatory function when responding to distal danger to its antimicrobial function upon encountering nearby threats. Class IIa HDACs can act via both enzyme-dependent and -independent mechanisms (27, 38). We therefore examined class IIa HDAC enzymatic activity in macrophages responding to *Escherichia coli*, finding that infection of BMM with UPEC resulted in a rapid increase in this response, with this abrogated in *Hdac7*-deficient BMM (*SI Appendix*, Fig. S5 *A* and *B*). Given this finding, we next assessed if HDAC7 enzymatic activity is required for macrophage antimicrobial responses by reconstituting a previously characterized enzyme-dead mutant of HDAC7, HDAC7ΔH649A (11), in *Hdac7*-deficient BMM (*SI Appendix*, Fig. S5*C*). Both phagocytosis of fluorescent *Escherichia coli* (*SI Appendix*, Fig. S5*D*) and *Escherichia coli* killing (*SI Appendix*, Fig. S5*E*) were significantly enhanced by wild-type but not enzyme-dead HDAC7. Furthermore, TMP195 did not increase *Escherichia coli* survival in *Hdac7*-deficient BMM (*SI Appendix*, Fig. S5*F*), thus confirming target specificity.

Having established enzyme dependence for the antimicrobial functions of HDAC7, we next investigated whether this function is linked to its role in immunometabolism, through inducible glycolysis (11) or the pentose phosphate pathway (Fig. 1*G*). Since glucose fuels both pathways, we investigated whether limiting glucose availability with 2-deoxy-D-glucose (2-DG) (39) impairs the antimicrobial functions of HDAC7. Indeed, this regime enhanced intramacrophage UPEC survival and abrogated the antimicrobial phenotype of Mac-Hdac7 BMM, such that intramacrophage bacterial survival was equivalent to MacBlue control BMM (*SI Appendix*, Fig. S5*G*). HDAC7 promotes LPS-inducible inflammatory responses by deacetylating the glycolytic enzyme PKM2 on K433 (11). Here, we found that DASA, which antagonizes proinflammatory functions of PKM2 (10) and HDAC7 (11), did not affect the antimicrobial functions of HDAC7

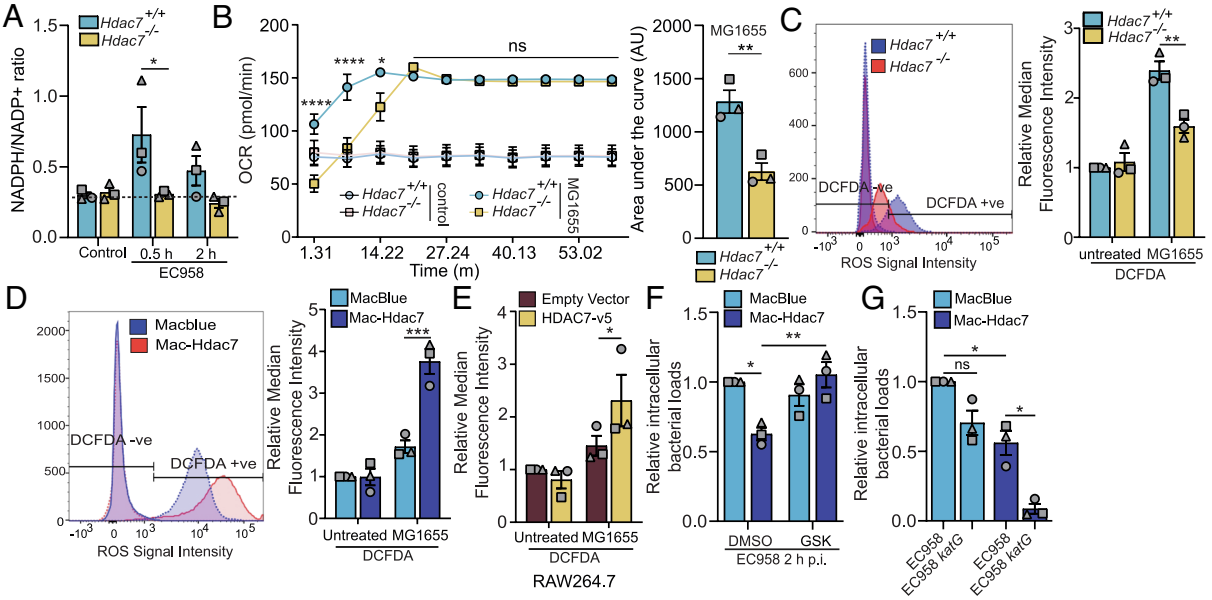

Fig. 4. Antimicrobial effects of HDAC7 require PPP- and NADPH oxidase-dependent ROS. (*A*) NADPH/NADP$^+$ ratio in the indicated BMM populations infected with EC958. (*B*) Measurement of real time OCR in the indicated BMM populations infected with MG1655 (*Left*). Area under the curve analysis until 15 min of OCR determinations was calculated with post-background correction (*Right*). (*C–E*) Measurement of total ROS in the indicated BMM populations (*C* and *D*) or RAW264.7 (*E*), pretreated with cM-H_2DCFDA (10 μM) for 30 min before infecting them with MG1655 for 30 min. Representative flow cytometry plot (*Left*), as well as relative median fluorescence intensity (MFI) data (*Right*), are shown for (*C* and *D*). (*F*) Relative intramacrophage EC958 loads at 2 h p.i. in indicated BMM populations, pretreated with the NOX2 inhibitor GSK2795039 (GSK, 10 μM) for 1 h. (*G*) Relative intramacrophage bacterial loads of EC958 or EC958*katG* at 2 h p.i. in the indicated BMM populations. Graphical data (mean ± SEM, n = 3) are combined from three independent experiments and are normalized to the *Hdac7*$^{+/+}$ uninfected control (*C*), uninfected MacBlue control (*D*), uninfected empty vector control (*E*), or MacBlue control infected with wild type EC958 (*F* and *G*). Statistical significance was determined using repeated measure two-way ANOVA followed by Sidak's multiple comparison test [*A* and *B* (*Left*)–*G*] or unpaired *t* test with Welch's correction [B (*Right*)] (ns, not significant; *P < 0.05; **P < 0.01; ***P < 0.001; ****P < 0.0001).

(*SI Appendix*, Fig. S5*G*). Using the same cells, we confirmed that both DASA and 2-DG blocked the capacity of HDAC7 to promote LPS-inducible IL-1β (*SI Appendix*, Fig. S5*H*) and that neither compound affected the viability of UPEC-infected macrophages (*SI Appendix*, Fig. S5*I*). Thus, the HDAC7-PKM2 pathway (11) is not involved in HDAC7 antimicrobial functions. Indeed, retroviral overexpression of either wild-type PKM2 or its hyperactive deacetylated mimic (PKM2-K433R) did not reduce intramacrophage bacterial loads (*SI Appendix*, Fig. S5*J*), whereas inflammasome-triggered IL-1β release in LPS-primed cells was amplified (*SI Appendix*, Fig. S5*K*), as expected (11). In summary, HDAC7 enzymatic activity is required for its capacity to promote bacterial phagocytosis and killing by macrophages, glucose uptake is required for the response, and the mechanism is distinct to the HDAC7-PKM2-IL-1β axis.

Antimicrobial Effects of HDAC7 Require PPP- and NADPH Oxidase-Dependent ROS. Professional phagocytes engage the respiratory burst to generate antimicrobial ROS (40). This rapid oxygen-consuming response (41) requires NADPH from the PPP (42). Since *Escherichia coli* triggered HDAC7-dependent PPP intermediate production in macrophages (Fig. 1*G*), we considered that HDAC7 may drive NADPH oxidase-dependent ROS for host defense. Consistent with this, the rapid *Escherichia coli*-mediated increase in the NADPH/NADP ratio in BMM required HDAC7 (Fig. 4*A*). Metabolic flux analysis also confirmed that rapid *Escherichia coli*-inducible oxygen consumption was significantly reduced in *Hdac7*-deficient macrophages (Fig. 4*B*), consistent with a defect in NADPH oxidase activity and the respiratory burst. Furthermore, *Escherichia coli*-inducible oxidative stress, as assessed by H_2DCFDA staining/flow cytometry, was significantly reduced in *Hdac7*-deficient BMM (Fig. 4*C*). Conversely, *Escherichia coli*-induced oxidative stress was enhanced in HDAC7 overexpressing Mac-Hdac7 BMM (Fig. 4*D*) and RAW 264.7 cells (Fig. 4*E*). Thus, HDAC7-mediated engagement of the PPP enables NADPH oxidase-dependent ROS production upon sensing proximal threats.

We next investigated whether ROS has a causal role in HDAC7-dependent antimicrobial effects. The NADPH oxidase inhibitor GSK2795039, which antagonized *Escherichia coli*-inducible oxidative stress (*SI Appendix*, Fig. S6*A*), blocked the antimicrobial phenotype of Mac-Hdac7 macrophages (Fig. 4*F*) without affecting cell viability (*SI Appendix*, Fig. S6*B*). In *Escherichia coli*, resistance to oxidative stress is conferred by a catalase-peroxidase (Hydroperoxidase I), a monofunctional catalase (Hydroperoxidase II), and an alkyl hydroxyperoxidase, which are encoded by *katG*, *katE*, and *ahpCF*, respectively (43, 44). KatG is important for scavenging peroxide at high H_2O_2 concentrations (44). To further examine the link between HDAC7-mediated ROS production and its antimicrobial effects, we generated a ROS-sensitive *katG* UPEC mutant (EC958*katG*). We predicted that this mutant would be susceptible to killing by Mac-Hdac7 macrophages that are primed to respond to proximal threats via ROS. As expected, the survival of wild-type EC958 was significantly reduced in Mac-Hdac7 BMM by comparison to control MacBlue BMM (Fig. 4*G*). Furthermore, intracellular survival of the EC958*katG* mutant was significantly reduced in Mac-Hdac7 macrophages in comparison to wild-type EC958, whereas there was only a modest reduction in its survival in control cells (Fig. 4*G*). Collectively, these data confirm that the PPP- and NADPH-dependent ROS production are required for HDAC7-mediated host defense in macrophages responding to proximal danger.

HDAC7 Interacts with and Activates 6PGD. We previously used a proteomics approach (45) to identify HDAC7-interacting partners in macrophages (11). Although that study focused on PKM2, the screen also identified the PPP enzyme 6PGD (peptide ELLPKIRDSAGQKGTGK: 6.52% protein coverage with 99% confidence). 6PGD, along with glucose-6-phosphate dehydrogenase (G6PD), generates NADPH for use by the phagocyte NADPH oxidase

to generate antimicrobial ROS (46). We thus considered 6PGD as a potential candidate for selective engagement of the PPP in macrophages responding to proximal versus distal danger. Indeed, treatment with LPS plus latex beads or infection with UPEC as surrogates of proximal danger rapidly upregulated 6PGD enzyme activity in BMM, whereas LPS or latex beads alone had no effect (Fig. 5*A*). This implicated 6PGD as a potential downstream target of HDAC7 in macrophages responding to proximal danger. Thus, we next investigated the HDAC7-6PGD interaction using coimmunoprecipitation assays. In HEK293T cells, 6PGD interacted with HDAC7, but not the class IIb HDAC, HDAC6 (Fig. 5*B*). Using a *Leishmania tarentolae* cell-free protein translation system (LTE) and AlphaLISA assays, we also confirmed that the interaction between HDAC7 and 6PGD is direct (Fig. 5*C*). Moreover, the nature of the interaction was distinct from that of HDAC7 with PKM2. 6PGD interacted with both the N-terminal and C-terminal domains of HDAC7, whereas PKM2 only interacted with the latter. The HDAC7-6PGD interaction was also more pronounced than that of HDAC7-PKM2 in cells, as assessed by coimmunoprecipitation assays (Fig. 5*D*). We next assessed whether HDAC7 regulates proximal danger-inducible 6PGD activity (Fig. 5*A*). Here, we found that *Hdac7* deletion (Fig. 5*E*) or pharmacological inhibition of HDAC7 with TMP195 attenuated UPEC-induced 6PGD activity in BMM (Fig. 5*F*) and primary human macrophages (Fig. 5*G*). Conversely, HDAC7 overexpression increased 6PGD enzymatic activity in transfected HEK293T cells (Fig. 5*H*), without affecting 6PGD protein levels (Fig. 5*I*). These data are consistent with HDAC7-mediated activation of 6PGD for antimicrobial ROS generation in macrophages responding to the proximal threat of a nearby bacterial pathogen.

HDAC7 Acts via the PPP Metabolite RL5P to Prioritize Responses to Proximal Danger Signals. Having established the role of HDAC7 in 6PGD activation, NADPH production, flux through the PPP, and ROS-dependent bacterial killing, we returned to our initial observation that HDAC7 limits IL-1β production in macrophages responding to proximal danger (Fig. 1 *B* and *D–F* and *SI Appendix*, Figs. S1*A* and S2 *A* and *D*). This inactivation of inflammatory responses might enable cells to focus resources on nearby threats. Given the preference for HDAC7 in interacting with 6PGD over PKM2 (Fig. 5*D*), we considered that bacterial challenge may trigger the HDAC7-6PGD antimicrobial response at the expense of the HDAC7-PKM2 inflammatory response. If so, HDAC7 overexpression should enhance IL-1β production even in cells responding to bacterial challenge. Indeed, this response was amplified in Mac-Hdac7 BMM responding to either LPS or UPEC (Fig. 6*A*), in stark contrast to our findings with the differential IL-1β response observed in *Hdac7*-deficient macrophages (Fig. 1 *D* and *E*). Next, we investigated whether HDAC7-mediated IL-1β suppression is linked to PPP engagement in macrophages responding to proximal danger. Here, we found that PPP inhibition with 6-aminonicotinamide (6-AN) or polydatin (PD) increased IL-1β in macrophages responding to UPEC (Fig. 6*B*). IL-1β levels in PPP-inhibited BMM were similar to those in *Hdac7*$^{-/-}$ BMM, and PPP inhibition did not further increase this response in *Hdac7*-deficient BMM. In contrast, UPEC-induced TNF was not affected by PPP inhibition or *Hdac7* deficiency (*SI Appendix*, Fig. S6*C*). This implicates the PPP in HDAC7-mediated inhibition of IL-1β in macrophages responding to proximal threats.

NADPH oxidase-mediated ROS production requires the PPP. Although ROS is implicated in NLRP3 inflammasome activation (47, 48), CGD patient cells that are defective in NADPH oxidase activity (49, 50) display heightened inflammasome activation and IL-1β release (16, 18). However, our findings are consistent with HDAC7 controlling inflammasome priming, rather than activation (Fig. 1*D* and *SI Appendix*, Fig. S1 *B* and *E*). Consistent with this, the NADPH oxidase inhibitor GSK2795039, which abrogated *Escherichia coli*-inducible ROS (*SI Appendix*, Fig. S6*A*), did not alter IL-1β production in wild-type or *Hdac7*$^{-/-}$ macrophages responding to LPS or UPEC (*SI Appendix*, Fig. S6 *D* and *E*). Similarly, GSK2795039 did not affect IL-1β release in the HDAC7 overexpression system (*SI Appendix*, Fig. S6 *F* and *G*). This suggests that NADPH oxidase-dependent ROS does not regulate IL-1β in this setting. We therefore investigated whether 6PGD itself regulates IL-1β, given that this PPP enzyme is activated by HDAC7 (Fig. 5 *E–H*). Indeed, *Pgd* silencing (*SI Appendix*, Fig. S6*H*) amplified inflammasome-triggered IL-1β release in LPS-primed BMM (Fig. 6*C*). As with earlier experiments examining HDAC7 functions in BMM (*SI Appendix*, Figs. S1*C* and S2*B*), inducible TNF production was unaffected by *Pgd* knockdown (*SI Appendix*, Fig. S6*I*). Consistent with these *Pgd* silencing data, ectopic expression of 6PGD in BMM attenuated inducible IL-1β (Fig. 6*D*). In this gain-of-function approach, 6PGD overexpression also significantly reduced LPS-induced TNF (*SI Appendix*, Fig. S6*J*). However, the effect of 6PGD was selective, since LPS-induced IL-6 was unaffected (*SI Appendix*, Fig. S6*K*). These experiments reveal that 6PGD serves a dual role during innate immune responses to proximal threats, providing NADPH to fuel phagocyte oxidase-mediated ROS production for bacterial killing and limiting inflammatory responses to enable cells to focus their resources on bacterial killing.

To further probe mechanisms by which 6PGD suppresses inflammatory responses, we examined RL5P, the enzymatic product of 6PGD. Remarkably, RL5P treatment suppressed LPS-inducible IL-1β in human and mouse macrophages (Fig. 6 *E* and *F*). In BMM, and to a lesser extent HMDM, this effect was much less pronounced in cells responding to UPEC. Thus, RL5P shows some selectively in attenuating inflammatory mediator production in macrophages responding to signals of distal versus proximal danger, likely because the PPP is already engaged in response to the latter. RL5P also reduced inducible TNF in macrophages (Fig. 6 *G* and *H*). In this case, RL5P dramatically reduced secreted TNF levels in HMDM, whereas the effect on BMM was modest and selective for responses to LPS versus *Escherichia coli*. These phenotypes are reminiscent of the more pronounced effects of HDAC7 inhibition on LPS-induced TNF in HMDM (Fig. 1*C*) by comparison to BMM (*SI Appendix*, Fig. S1*D*), as well as the effect of 6PGD overexpression on LPS-induced TNF in BMM (*SI Appendix*, Fig. S6*J*). However, antiinflammatory effects of RL5P in both HMDM and BMM were selective, since this metabolite did not affect inducible IL-6 in response to either distal or proximal threats (*SI Appendix*, Fig. S7 *A* and *B*). Thus, HDAC7-dependent RL5P production suppresses specific inflammatory responses in macrophages responding to proximal threats.

The RL5P-producing enzyme 6PGD can physically interact with and regulate the phagocyte oxidase (51, 52), so it is conceivable that bacteria in the phagosome being subjected to oxidative stress may also encounter RL5P. We thus considered that this metabolite may exert direct antimicrobial effects, particularly in the presence of ROS. Here, we found that when UPEC were grown in a concentration of hydrogen peroxide that minimally affected bacterial growth (0.8 mM H_2O_2), RL5P significantly attenuated UPEC growth in a dose-dependent manner (Fig. 6*I* and *SI Appendix*, Fig. S7*C*). This effect was also apparent for UPEC cultured with 1 mM H_2O_2 that dramatically impaired bacterial growth (*SI Appendix*, Fig. S7*D*). Importantly, RL5P did not affect UPEC growth in the absence of oxidative stress (*SI Appendix*, Fig. S7*E*). Furthermore, in contrast to RL5P, the upstream PPP metabolite and 6PGD substrate, 6-phosphogluconate (6PG), did not affect UPEC growth in the presence of H_2O_2 (Fig. 6*J* and

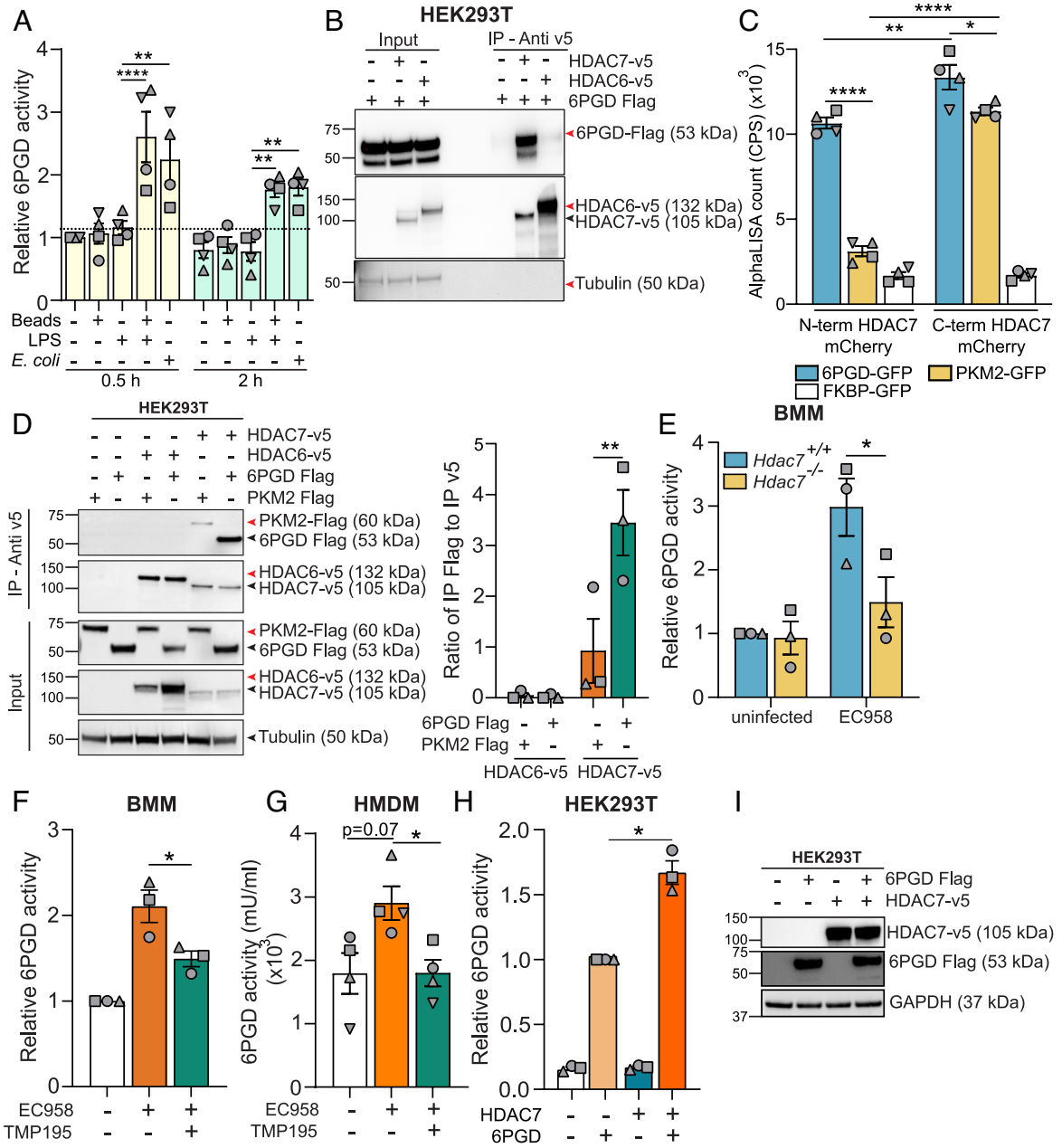

Fig. 5. HDAC7 interacts with and activates 6PGD. (*A*) 6PGD activity assay on lysates from BMM that had been treated for 0.5 h or 2 h with either LPS (1 ng/mL), latex beads, or LPS plus latex beads or infected with EC958 (MOI 100). (*B*) Immunoblot of coimmunoprecipitation assay using HEK293T lysates to assess 6PGD interactions (representative of three independent experiments). (*C*) AlphaLISA assay to analyze the interaction between HDAC7 and 6PGD, PKM2, or FKBP (negative control) following cell-free expression of indicated proteins. (*D*) Immunoblot (representative of three independent experiments, *Left*) of coimmunoprecipitation assay using HEK293T lysates to assess strength of HDAC7 interaction with target proteins (6PGD versus PKM2). Interactions were quantified by densitometric analysis of FLAG-tagged proteins (*Right*). (*E*) 6PGD activity assay on lysates from the indicated BMM populations infected with EC958 for 2 h. (*F* and *G*) 6PGD activity assay on lysates from BMM (*F*) or HMDM (*G*) pretreated with TMP195 (10 μM) for 1 h followed by infection with EC958 for 2 h. (*H* and *I*) 6PGD activity assay on lysates from HEK293T cells cotransfected with the indicated constructs (*H*). Immunoblotting was performed on the lysates to confirm similar expression of the proteins (*I*, representative of three independent experiments). Graphical data (mean ± SEM, n = 3 to 4) are combined from at least three independent experiments and are normalized to untreated control (*A*), *Hdac7*$^{+/+}$ uninfected control (*E*), uninfected control (*F*), or 6PGD alone (*H*). 6PGD enzyme activity was normalized to the total protein in the lysate (*A*, *E*–*G*). Statistical significance was determined using two-way ANOVA (*A* and *C*–*E*), repeated measure one-way ANOVA with Giesser Greenhouse correction (*F* and *H*), or nonparametric Kruskal–Wallis test (*G*) followed by Tukey's, Dunn's, Dunnett's, or Sidak's multiple comparison test (ns, not significant; *$P < 0.05$; **$P < 0.01$; ****$P < 0.0001$).

SI Appendix, Fig. S7*F*). These data thus implicate RL5P in oxidative stress-mediated antimicrobial responses in macrophages. In summary, our study supports a model in which HDAC7 can coopt the glycolytic enzyme PKM2 to drive inflammatory responses upon sensing distal threats, as well as instruct both antimicrobial defense via 6PGD-NADPH-ROS/RL5P and inflammation suppression via 6PGD-RL5P upon encountering the threat of nearby bacteria (*SI Appendix*, Fig. S8).

Discussion

Here, we reveal that HDAC7 in macrophages triages incoming danger signals, functioning as an immunometabolic switch for context-dependent control of inflammatory and antimicrobial pathways (*SI Appendix*, Fig. S8). Upon encountering the proximal threat of UPEC, HDAC7 engages 6PGD in the anabolic PPP to switch on ROS-dependent bacterial killing and switch off proinflammatory IL-1β. Remarkably, two metabolites generated by

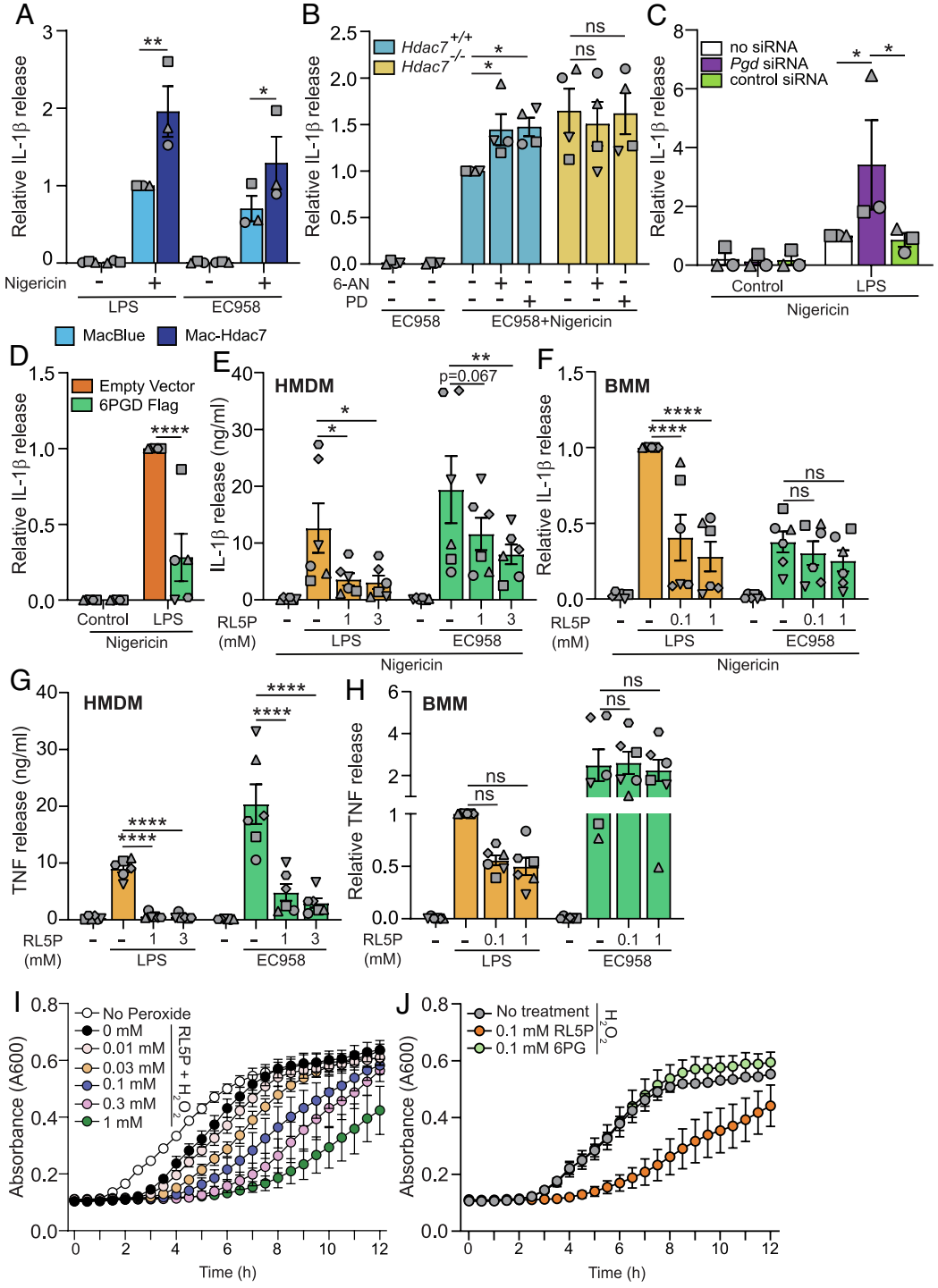

Fig. 6. HDAC7 acts via the PPP metabolite RL5P to prioritize responses to proximal danger signals. (*A*) IL-1β release from the indicated BMM populations infected with either EC958 (MOI 10) or treated with LPS (100 ng/mL) for 4 h, followed by an additional treatment with nigericin for 1 h. (*B*) IL-1β release from the indicated BMM populations pretreated with the PPP inhibitors 6-aminonicotinamide (6-AN) (0.5 μM) or polydatin (PD) (0.5 μM) for 1 h, followed by infection with EC958 for 4 h. Additional nigericin treatment for 1 h followed. (*C*) IL-1β release from BMM knocked down for the indicated genes, treated with LPS (0.5 ng/mL) for 4 h followed by nigericin treatment for 1 h. (*D*) IL-1β release from BMM retrovirally transduced with indicated constructs, treated with LPS (0.5 ng/mL) for 4 h followed by an additional treatment with nigericin for 1 h. (*E–H*) IL-1β and TNF release from HMDM and BMM pretreated with the indicated concentrations of ribulose-5-phosphate for 16 h, followed by LPS (10 ng/mL) or infection with EC958 for 4 h. Additional treatment with nigericin for 1 h followed. (*I* and *J*) Growth curve analysis (A_{600}) of EC958 cultured ± H_2O_2 (0.8 mM) in the presence of the indicated concentrations of RL5P (*I*) or 6-phosphogluconate (6PG) (*J*) for 12 h. All graphical data (mean ± SEM, n = 3 to 6) are combined from three to six independent experiments unless otherwise specified and are normalized to the MacBlue (*A*), *Hdac7*$^{+/+}$ (*B*), LPS-treated no siRNA control (*C*), LPS-treated empty vector control (*D*), or LPS-treated BMMs (*F, H*). Statistical significance was determined using repeated measure two-way ANOVA followed by Sidak's, or Dunnett's multiple comparison test (*A–H*) (ns, not significant; *$P < 0.05$; **$P < 0.01$; ****$P < 0.0001$).

6PGD appear to be deployed for this context-dependent response to nearby danger. NADPH fuels the phagocyte oxidase system for antimicrobial ROS while RL5P serves dual roles, enhancing ROS-mediated antibacterial defense and selectively dampening inflammatory responses. The triggering of this pathway by HDAC7 contrasts with its proinflammatory function in cells responding to soluble danger signals such as LPS, where it uses the glycolytic enzyme PKM2 to promote IL-1β production (11). This coopting

of distinct metabolic enzymes by HDAC7 provides a means of rapidly directing resources toward proinflammatory versus antibacterial responses. It also enables HDAC7 to prioritize danger signals, focusing efforts on bacterial killing when proximal threats are encountered. The biological significance of this is highlighted by our observations that targeting of HDAC7 dampens LPS-induced inflammation in vivo (11) but exacerbates inflammatory responses during bacterial infection (Fig. 3). The interplay between glycolysis and the PPP in macrophages is reminiscent of a recent study showing that selective engagement of glycolysis dampened flux through the PPP, reducing NADPH oxidase-dependent outputs in neutrophils (53).

Our discovery of immunomodulatory and antimicrobial effects of the 6PGD product RL5P (Fig. 6 *E–J* and *SI Appendix*, Fig. S7) provides an avenue for exploiting the PPP to dampen inflammation without compromising host defense, for example, through RL5P or RL5P analogs in inflammatory conditions. How RL5P exerts its immunomodulatory effects, for example, through receptor-mediated signaling and/or direct inhibition of inflammatory gene expression, remains an exciting question for the future. Interestingly, 6PGD is required for T regulatory cell functions (54), so it is possible that RL5P also contributes to the immunosuppressive functions of these cells and in controlling immune responses. Mechanisms by which RL5P limits bacterial growth is also an open question. This PPP metabolite only impaired bacterial growth in UPEC experiencing oxidative stress (Fig. 6 *I* and *J* and *SI Appendix*, Fig. S7*E*). The PPP, and ribulose-5-phosphate 3-epimerase in particular, is susceptible to poisoning by H_2O_2 in *Escherichia coli* (55). One possibility, therefore, is that RL5P sensitizes UPEC to ROS-mediated inactivation of the PPP. Another is that oxidative stress enables RL5P or a downstream metabolite to exert direct antimicrobial effects. Whatever the mechanisms, our data suggest that 6PGD and RL5P may be important players in ROS-mediated host defense. It will thus be of interest to characterize the spectrum of bacterial species that are sensitive to RL5P.

The importance of PPP-derived NADPH in host defense is exemplified by its link to the phagocyte NADPH oxidase and CGD. The PPP is required for NADPH generation to fuel the enzymatic function of the phagocyte oxidase (21), with genetic deficiencies in this enzyme complex leading to recurrent life-threatening infections (15). More direct links between the PPP and host defense have long been appreciated. A patient with complete deficiency in the PPP enzyme G6PD succumbed to fatal sepsis, with impaired bactericidal activity being noted in their leukocytes (56). A similar CGD-like phenotype was observed in another individual with complete G6PD deficiency (57) and several others have more recently been reported (58). These rare, severe immunodeficiencies contrast with more common genetic defects in which G6PD function is not completely defective and that generally does not compromise innate immune defense, instead predisposing to haemolytic anaemia (59). As with G6PD, 6PGD also generates NADPH that fuels the phagocyte oxidase to generate ROS (60), but its role in host defense has been explored in only a limited way. 6PGD was identified as a component of the active phagocyte NADPH oxidase complex in neutrophils (61), promoting both NADPH binding to the phagocyte oxidase and its enzymatic activity (52). Our demonstration that bacterial infection increases 6PGD enzymatic activity via HDAC7 in mouse (Fig. 5 *E* and *F*) and human macrophages (Fig. 5*G*) suggests that this may be a key regulatory mechanism for switching on NADPH oxidase-dependent ROS in macrophages and, potentially, neutrophils. Certainly, several lines of evidence from our study link HDAC7 to NADPH oxidase-dependent ROS production in macrophages. These include host genetic data revealing HDAC7 involvement in *Escherichia coli*-inducible NADPH production (Fig. 4*A*), rapid oxygen consumption (Fig. 4*B*), and acute oxidative stress (Fig. 4 *C–E*); bacterial genetic data linking a ROS-sensitive UPEC mutant to HDAC7-mediated killing (Fig. 4*G*); and pharmacological data demonstrating that NADPH oxidase is required for HDAC7-mediated bacterial killing (Fig. 4*F*).

HDAC7 and other members of the class IIa HDAC family are often considered as inactive enzymes (62). This view is challenged by recent demonstrations that LPS rapidly activates HDAC7 enzymatic activity in macrophages (29) and that this is necessary for driving production of specific proinflammatory mediators (11, 29). Here, we reveal that UPEC infection of murine macrophages also activated HDAC7 enzymatic activity (*SI Appendix*, Fig. S5*B*), with this promoting both phagocytosis (*SI Appendix*, Fig. S5*D*) and bacterial killing (*SI Appendix*, Fig. S5*E*). Given that HDAC7 also instructs inflammatory responses via deacetylation of PKM2 (11), this lysine deacetylase is emerging as a key player in macrophage metabolism, inflammation, and host defense. Our findings therefore challenge the widely held view that class IIa HDAC proteins lack enzymatic activity in cells. Whether HDAC7 enzymatic activity is required for PPP activation and ROS production in macrophages responding to proximal threats is unknown. The enzymatic activities of both G6PD and 6PGD are regulated by lysine acetylation. For example, acetylation at K403 deactivates G6PD in HEK293T cells (63), whilst acetylation at K74 and K294 enhances 6PGD activity in H1299 cells (64). Interestingly, a constitutively deacetylated form of 6PGD was associated with an enhanced ROS response (64). It is therefore possible that HDAC7-mediated deacetylation of 6PGD in macrophages is essential for generating ROS, consistent with our findings linking HDAC7 to inducible ROS and ROS-dependent bacterial killing (Fig. 4 *B–G*). This would fit with the observation that HDAC7 enzymatic activity is required for its antimicrobial functions (*SI Appendix*, Fig. S5*E*). However, it is also possible that HDAC7 regulates 6PGD via non-enzymatic mechanisms, with the antimicrobial effects of HDAC7 enzymatic activity being a consequence of phagocytosis-mediated host defense.

Although ROS is often considered a culprit in acute and chronic disease, NADPH oxidase-generated ROS can limit inflammation-mediated pathology in some circumstances. For example, superoxide inhibits caspase-1 function through cysteine oxidation (65), with mononuclear cells from CGD patients displaying enhanced caspase-1 activation and IL-1β release (16). Dysregulated inflammasome responses are thought to contribute to inflammation-associated clinical manifestations, such as colitis, in CGD patients (66). Initially, our characterization of the HDAC7-PPP-6PGD axis seemed to be consistent with this NADPH oxidase-dependent constraint of inflammasome responses via ROS. However, NADPH oxidase inhibition did not influence HDAC7-mediated control of IL-1β (*SI Appendix*, Fig. S6 *D–G*). Given that HDAC7 constrains *Escherichia coli*-inducible IL-1β through the PPP (Fig. 6*B*), this suggests an additional ROS-independent mechanism of regulatory control by this pathway. Consistent with this, methionine and S-adenosylmethionine both enhance the PPP and inhibit inflammatory responses (67–69). Our studies support a common mechanism by which HDAC7-mediated PPP activation both promotes ROS production and constrains IL-1β, namely via 6PGD. Given that 6PGD interacts with and regulates the phagocyte NADPH oxidase (52, 61), it will be of interest to determine whether defective 6PGD localization and/or function contributes to the excessive IL-1β response and inflammation-associated pathology characteristic of CGD patients (70). Our findings may also have broader implications for understanding inflammation-driven

disease. Given the central role of IL-1β in driving pathology in many conditions (71), 6PGD agonists, RL5P analogs, and/or activators of the HDAC7-6PGD pathway may have potential in antiinflammatory drug development.

Our discovery of the HDAC7-6PGD axis also has implications for targeting HDAC7 in other disease contexts. 6PGD contributes to tumor growth and metastasis in many cancers (60, 72) and constrains anti-tumor responses of CD8 T cells (73). Thus, HDAC7 antagonists may offer an alternative approach to target 6PGD for anticancer applications. Interestingly, inhibition of class IIa HDACs reduced tumor burden and metastasis in a mouse breast cancer model (74). This was attributed to the recruitment of anti-tumor macrophages, but it is possible that PPP inhibition also contributes to the anticancer effects of inhibitors of class IIa HDACs. In contrast to its potential role in limiting inflammatory disease pathology in CGD patients, NADPH oxidase-dependent ROS is implicated in tissue damage in other circumstances. For instance, *Nox2*-deficient mice were protected against TNF-induced lung inflammation (75), sepsis-induced lung microvascular injury (76), pulmonary fibrosis (77), and atherosclerotic lesions (78). Thus, targeting HDAC7 in these contexts may limit pathology by attenuating proinflammatory ROS production.

In summary, we establish a unique, context-dependent role for HDAC7 in regulating macrophage functions upon encountering proximal threats, identifying 6PGD as a downstream target that both engages host defense through one of its enzymatic products (NADPH) and limits inflammatory responses through another (RL5P). We propose that this dual functionality of 6PGD in generating both NADPH to fuel phagocyte oxidase-mediated ROS and RL5P for inhibition of inflammatory mediators may enable host cells to focus their resources on direct microbial destruction rather than on energy-demanding immune cell recruitment during early responses to infection. Moreover, our characterization of the HDAC7-6PGD-RL5P axis identifies an upstream control point for directing inflammatory versus antimicrobial responses in innate immune cells, a finding that may be amenable to antiinfective and/or antiinflammatory strategies.

Materials and Methods

Ethics Statement. All animal studies were approved by the appropriate University of Queensland animal ethics committee (IMB/123/18, IMB/118/15, IMB/118/18, IMB/121/15, and IMB/327/17). Human peripheral blood was collected from healthy donors following informed consent, after which mononuclear cells were isolated, as described in *SI Appendix*, *Supplementary Materials and Methods*. All experiments that involved the isolation and functional analyses of these cells were approved by The University of Queensland Institutional Human Research Ethics Committee.

Animals. Male and female C57BL/6J mice of 8 to 12 wk of age were obtained from an in-house breeding colony within the QBP animal house (The University of Queensland) or from the animal resources centre (Murdoch, WA). Mac-Hdac7 mice, which overexpress HDAC7 in myeloid cells, have previously been described (11). Littermate MacBlue mice expressing cyan fluorescent protein (CFP) in myeloid cells (79) were used as controls for studies using Mac-Hdac7 mice. Myeloid-deleted *Hdac7* mice ($Hdac7^{-/-}$) (11) were obtained by crossing $Hdac7^{flox/flox}$/$LysM^{Cre}$ mice with $Hdac7^{flox/flox}$ mice, with littermate $Hdac7^{flox/flox}$ ($Hdac7^{+/+}$) mice used as controls (80). As an additional control to ensure that the $LysM^{Cre}$ allele did not confound data interpretation, functional assays (IL-1β release by ELISA, *Escherichia coli*-induced ROS production, and intracellular UPEC loads in macrophages) were performed to compare the phenotypes of BMM from $LysM^{Cre}$, $Hdac7^{+/+}$, and $Hdac7^{-/-}$ mice (*SI Appendix*, Fig. S9 *A–D*). $Tlr4^{-/-}$ mice (81) were maintained on a C57BL/6J background at the QBP animal house.

In Vivo Studies. C57BL/6J mice were administered with 50 mg/kg TMP195 or vehicle (DMSO) for 1 h and then *i.p.* infected with EC958 (2×10^6 CFU in 100 μL). Alternatively, $Hdac7^{flox/flox}$/$LysM^{Cre}$ ($Hdac7^{-/-}$) and $Hdac7^{flox/flox}$ littermate control mice ($Hdac7^{+/+}$) were *i.p.* infected with UPEC strain EC958 (2×10^6 CFU). At indicated time points, the core body temperature was recorded using a rectal thermometer (Warner Instruments, Cat – 64-1654). Mice were euthanized at 8 h post-challenge, after which peritoneal exudates, livers, and spleens were collected. Peritoneal exudates were centrifuged and lysed using PBS containing 0.01% Triton X-100. To determine bacterial loads in the spleen and liver, organs were homogenized in 1 mL PBS utilizing a T10 Ultra Turrax homogenizer (spleen: speed 3, 15 s; liver: speed 4, 1 min). Triton X-100 was added to a final concentration of 0.1%, with homogenates plated overnight on ampicillin (100 mg/mL)-containing LB plates to determine CFU per organ.

Statistical Analysis. Where statistical analyses were performed, data were combined from three or more independent experiments, with each experiment designated by a different symbol. In the case of experiments on primary human macrophages, each experiment also used cells from a different donor. Statistical analyses were performed using Prism 8 software (Graph-Pad) with error bars indicating the SEM or interquartile range. Details of statistical tests are provided in *SI Appendix*, Supplementary Methods.

Detailed Methodologies. Details of all chemicals and reagents, along with detailed methodologies (bacterial and mammalian cell culture, gene expression analysis, cytokine analysis, biochemical assays, metabolomic analysis, infection assays, and analysis of ROS production and phagocytic uptake of bacteria), are provided in *SI Appendix*, Supplementary Methods.

Data, Materials, and Software Availability. All study data are included in the article and/or *SI Appendix*.

ACKNOWLEDGMENTS. This work was supported by an Australian Research Council (ARC) Discovery Project (DP170102321 to M.J.S.), a National Health and Medical Research Council of Australia (NHMRC) Project Grant (APP1047921 to A.I., D.P.F., and M.J.S.), and an NHMRC Ideas Grant (APP1184885 to D.R. and M.J.S.). M.J.S. is supported by an NHMRC Investigator grant (APP1194406), D.P.F. acknowledges an NHMRC Senior Principal Research Fellowship (APP1117017) as well as an NHMRC Investigator grant (APP2009551), and M.R.S. and A.I. were supported by University of Queensland Postdoctoral Fellowships. L.L. was supported by ARC DECRA Fellowship (DE180100524). J.L.S. and K.S. are supported by NHMRC Investigator Grants APP1176209 and APP2009075, respectively. We acknowledge the Institute for Molecular Bioscience Dynamic Imaging Facility for Cancer Biology at The University of Queensland, established with the support of the Australian Cancer Research Foundation; the IMB Mass Spectrometry Facility; the Transgenic Animal Facility of Queensland (a division of The University of Queensland Biological Resources department); and the ARC Centre of Excellence in Advanced Molecular Imaging (CE140100011). Metabolomics Australia is part of the Bioplatforms Australia network, funded through the Australian Government's National Collaborative Research Infrastructure Strategy (NCRIS). We thank Prof. Eric Olson and Prof. Rhonda Bassel-Duby for providing $Hdac7^{fl/fl}$ mice (UT Southwestern Medical Centre).

Author affiliations: [a]Institute for Molecular Bioscience, Institute for Molecular Bioscience Centre for Inflammation and Disease Research, and Australian Infectious Diseases Research Centre, The University of Queensland, Brisbane, QLD 4072, Australia; [b]School of Chemistry and Molecular Biosciences, and Australian Infectious Diseases Research Centre, The University of Queensland, Brisbane, QLD 4072, Australia; [c]The Commonwealth Scientific and Industrial Research Organisation-Queensland University of Technology Synthetic Biology Alliance, Australian Research Council Centre of Excellence in Synthetic Biology, School of Biology and Environmental Science, Queensland University of Technology, Brisbane, QLD 4001, Australia; [d]Department of Internal Medicine, Inflammation Program, Roy J. and Lucille A. Carver College of Medicine University of Iowa, Iowa City, IA 52242; and [e]Metabolomics Australia (Queensland Node), Australian Institute for Bioengineering and Nanotechnology, The University of Queensland, Brisbane, QLD 4072, Australia

Author contributions: K.D.G., M.R.S., M.J.S. designed research; K.D.G., D.R., J.B.v.P., J.E.B.C., Y.W., R.A., S.V.M., K.S.G., A.M.V.M., C.J.S., R.K., Z.C.I., M.P., L.L., D.K. performed research; K.D.G., A.K., R.C.R., A.I., W.M.N., M.P., K.S., M.A.S., M.J.S. contributed new reagents/analytic tools; K.D.G., D.R., J.B.v.P., J.E.B.C., Y.W., R.A., S.V.M., K.S.G., A.M.V.M., C.J.S., L.L. analyzed data; K.D.G., D.R., R.K., J.L.S., D.K., K.A., M.R.S., M.A.S., D.P.F., M.J.S. supervision; K.D.G., D.R., R.A., S.V.M., A.M.V.M., C.J.S., W.M.N., M.P., L.L., J.L.S., K.S., D.K., M.A.S., D.P.F., M.J.S. review and editing; D.R., A.I., D.P.F., M.J.S. funding acquisition; and K.D.G. and M.J.S. wrote the paper.

1. K. A. Fitzgerald, J. C. Kagan, Toll-like receptors and the control of immunity. *Cell* **180**, 1044–1066 (2020).
2. B. Beutler, TLR4 as the mammalian endotoxin sensor. *Curr. Top. Microbiol. Immunol.* **270**, 109–120 (2002).
3. N. Kayagaki *et al.*, Non-canonical inflammasome activation targets caspase-11. *Nature* **479**, 117–121 (2011).
4. P. J. Baker *et al.*, NLRP3 inflammasome activation downstream of cytoplasmic LPS recognition by both caspase-4 and caspase-5. *Eur. J. Immunol.* **45**, 2918–2926 (2015).
5. R. D. Klein, S. J. Hultgren, Urinary tract infections: Microbial pathogenesis, host-pathogen interactions and new treatment strategies. *Nat. Rev. Microbiol.* **18**, 211–226 (2020).
6. T. Kawai, S. Akira, Signaling to NF-kappaB by Toll-like receptors. *Trends Mol. Med.* **13**, 460–469 (2007).
7. M. R. Shakespear *et al.*, Lysine deacetylases and regulated glycolysis in macrophages. *Trends Immunol.* **39**, 473–488 (2018).
8. M. A. Lauterbach *et al.*, Toll-like receptor signaling rewires macrophage metabolism and promotes histone acetylation via ATP-citrate lyase. *Immunity* **51**, 997–1011.e1017 (2019).
9. T. Shirai *et al.*, The glycolytic enzyme PKM2 bridges metabolic and inflammatory dysfunction in coronary artery disease. *J. Exp. Med.* **213**, 337–354 (2016).
10. E. M. Palsson-McDermott *et al.*, Pyruvate kinase M2 regulates Hif-1alpha activity and IL-1beta induction and is a critical determinant of the warburg effect in LPS-activated macrophages. *Cell Metabol.* **21**, 65–80 (2015).
11. K. Das Gupta *et al.*, Class iia histone deacetylases drive toll-like receptor-inducible glycolysis and macrophage inflammatory responses via pyruvate kinase M2. *Cell Rep.* **30**, 2712–2728.e8 (2020).
12. M. J. Sweet, N. J. Bokil, "chap. 1" in *Regulation of Innate Immune Function*, S. T. Clay, B. Marsh, Eds. (Research Signpost, Trivandrum, 2010), pp. 1–31.
13. R. S. Flannagan, G. Cosio, S. Grinstein, Antimicrobial mechanisms of phagocytes and bacterial evasion strategies. *Nat. Rev. Microbiol.* **7**, 355–366 (2009).
14. W. M. Nauseef, The phagocyte NOX2 NADPH oxidase in microbial killing and cell signaling. *Curr. Opin. Immunol.* **60**, 130–140 (2019).
15. E. Song *et al.*, Chronic granulomatous disease: A review of the infectious and inflammatory complications. *Clin. Mol. Allergy* **9**, 10 (2011).
16. F. Meissner *et al.*, Inflammasome activation in NADPH oxidase defective mononuclear phagocytes from patients with chronic granulomatous disease. *Blood* **116**, 1570–1573 (2010).
17. Y. F. Huang *et al.*, Redox regulation of pro-IL-1β processing may contribute to the increased severity of serum-induced arthritis in NOX2-deficient mice. *Antioxid. Redox Signal.* **23**, 973–984 (2015).
18. F. L. van de Veerdonk *et al.*, Reactive oxygen species–independent activation of the IL-1β inflammasome in cells from patients with chronic granulomatous disease. *Proc. Natl. Acad. Sci. U.S.A.* **107**, 3030–3033 (2010).
19. G. Angelino *et al.*, Inflammatory bowel disease in chronic granulomatous disease: An emerging problem over a twenty years' experience. *Pediatr. Allergy Immunol.* **28**, 801–809 (2017).
20. F. Imanzade, A. Sayarri, P. Tajik, Ulcerative colitis associated with chronic granulomatous disease: Case report. *Gastroenterol. Hepatol. Bed Bench* **8**, 233–235 (2015).
21. J. M. Ghergurovich *et al.*, A small molecule G6PD inhibitor reveals immune dependence on pentose phosphate pathway. *Nat. Chem. Biol.* **16**, 731–739 (2020).
22. E. C. Britt *et al.*, Switching to the cyclic pentose phosphate pathway powers the oxidative burst in activated neutrophils. *Nat. Metab.* **4**, 389–403 (2022).
23. C. Choudhary *et al.*, Lysine acetylation targets protein complexes and co-regulates major cellular functions. *Science* **325**, 834–840 (2009).
24. S. Zhao *et al.*, Regulation of cellular metabolism by protein lysine acetylation. *Science* **327**, 1000–1004 (2010).
25. M. R. Shakespear, M. A. Halili, K. M. Irvine, D. P. Fairlie, M. J. Sweet, Histone deacetylases as regulators of inflammation and immunity. *Trends Immunol.* **32**, 335–343 (2011).
26. M. Parra, Class IIa HDACs – new insights into their functions in physiology and pathology. *FEBS J.* **282**, 1736–1744 (2015).
27. Y. Wang *et al.*, Histone deacetylase 7: A signalling hub controlling development, inflammation, metabolism and disease. *FEBS J.*, in press (2022).
28. M. M. Mihaylova *et al.*, Class IIa histone deacetylases are hormone-activated regulators of FOXO and mammalian glucose homeostasis. *Cell* **145**, 607–621 (2011).
29. D. Ramnath *et al.*, The histone deacetylase Hdac7 supports LPS-inducible glycolysis and Il-1β production in murine macrophages via distinct mechanisms. *J. Leukoc. Biol.* **111**, 327–336 (2022).
30. M. Lobera *et al.*, Selective class IIa histone deacetylase inhibition via a nonchelating zinc-binding group. *Nat. Chem. Biol.* **9**, 319–325 (2013).
31. P. Millet, V. Vachharajani, L. McPhail, B. Yoza, C. E. McCall, GAPDH binding to TNF-α mRNA contributes to posttranscriptional repression in monocytes: A novel mechanism of communication between inflammation and metabolism. *J. Immunol.* **196**, 2541–2551 (2016).
32. A. H. Chan, K. Schroder, Inflammasome signaling and regulation of interleukin-1 family cytokines. *J. Exp. Med.* **217**, e20190314 (2020).
33. K. Schroder *et al.*, Conservation and divergence in Toll-like receptor 4-regulated gene expression in primary human versus mouse macrophages. *Proc. Natl. Acad. Sci. U.S.A.* **109**, E944–E953 (2012).
34. G. M. Tannahill *et al.*, Succinate is an inflammatory signal that induces IL-1β through HIF-1α. *Nature* **496**, 238–242 (2013).
35. M. Nagl *et al.*, Phagocytosis and killing of bacteria by professional phagocytes and dendritic cells. *Clin. Diagn. Lab. Immunol.* **9**, 1165–1168 (2002).
36. M. R. Shakespear *et al.*, Histone deacetylase 7 promotes Toll-like receptor 4-dependent proinflammatory gene expression in macrophages. *J. Biol. Chem.* **288**, 25362–25374 (2013).
37. A. Garami, A. A. Steiner, A. A. Romanovsky, Fever and hypothermia in systemic inflammation. *Handb. Clin. Neurol.* **157**, 565–597 (2018).
38. M. Martin, R. Kettmann, F. Dequiedt, Class IIa histone deacetylases: Regulating the regulators. *Oncogene* **26**, 5450–5467 (2007).
39. H. I. Nakada, A. N. Wick, The effect of 2-deoxyglucose on the metabolism of glucose, fructose, and galactose by rat diaphragm. *J. Biol. Chem.* **222**, 671–676 (1956).
40. B. M. Babior, NADPH oxidase: An update. *Blood* **93**, 1464–1476 (1999).
41. B. C. VanderVen, R. M. Yates, D. G. Russell, Intraphagosomal measurement of the magnitude and duration of the oxidative burst. *Traffic* **10**, 372–378 (2009).
42. K. C. Patra, N. Hay, The pentose phosphate pathway and cancer. *Trends Biochem. Sci.* **39**, 347–354 (2014).
43. P. C. Loewen, J. Switala, B. L. Triggs-Raine, Catalases HPI and HPII in Escherichia coli are induced independently. *Arch. Biochem. Biophys.* **243**, 144–149 (1985).
44. L. C. Seaver, J. A. Imlay, Alkyl hydroperoxide reductase is the primary scavenger of endogenous hydrogen peroxide in Escherichia coli. *J. Bacteriol.* **183**, 7173–7181 (2001).
45. H. Mohammed *et al.*, Rapid immunoprecipitation mass spectrometry of endogenous proteins (RIME) for analysis of chromatin complexes. *Nat. Protoc.* **11**, 316–326 (2016).
46. L. Jin, Y. Zhou, Crucial role of the pentose phosphate pathway in malignant tumors (Review). *Oncol. Lett.* **17**, 4213–4221 (2019).
47. C. Dostert *et al.*, Innate immune activation through Nalp3 inflammasome sensing of asbestos and silica. *Science* **320**, 674–677 (2008).
48. L. Franchi, T. Eigenbrod, R. Munoz-Planillo, G. Nunez, The inflammasome: A caspase-1-activation platform that regulates immune responses and disease pathogenesis. *Nat. Immunol.* **10**, 241–247 (2009).
49. D. B. Kohn *et al.*, Lentiviral gene therapy for X-linked chronic granulomatous disease. *Nat. Med.* **26**, 200–206 (2020).
50. G. Anjani *et al.*, Recent advances in chronic granulomatous disease. *Genes Dis.* **7**, 84–92 (2020).
51. M.-H. Paclet, S. Berthier, L. Kuhn, J. Garin, F. Morel, Regulation of phagocyte NADPH oxidase activity: Identification of two cytochrome b558 activation states. *FASEB J.* **21**, 1244–1255 (2007).
52. A. Baillet *et al.*, Coupling of 6-phosphogluconate dehydrogenase with NADPH oxidase in neutrophils: Nox2 activity regulation by NADPH availability. *FASEB J.* **25**, 2333–2343 (2011).
53. N. Amara *et al.*, Selective activation of PFKL suppresses the phagocytic oxidative burst. *Cell* **184**, 4480–4494.e15 (2021).
54. S. Daneshmandi, T. Cassel, R. M. Higashi, T. W. Fan, P. Seth, 6-Phosphogluconate dehydrogenase (6PGD), a key checkpoint in reprogramming of regulatory T cells metabolism and function. *Elife* **10**, e67476 (2021).
55. J. M. Sobota, J. A. Imlay, Iron enzyme ribulose-5-phosphate 3-epimerase in *Escherichia coli* is rapidly damaged by hydrogen peroxide but can be protected by manganese. *Proc. Natl. Acad. Sci. U.S.A.* **108**, 5402–5407 (2011).
56. M. R. Cooper *et al.*, Complete deficiency of leukocyte glucose-6-phosphate dehydrogenase with defective bactericidal activity. *J. Clin. Invest.* **51**, 769–778 (1972).
57. G. R. Gray *et al.*, Neutrophil dysfunction, chronic granulomatous disease, and non-spherocytic haemolytic anaemia caused by complete deficiency of glucose-6-phosphate dehydrogenase. *Lancet* **2**, 530–534 (1973).
58. D. Roos *et al.*, Hematologically important mutations: X-linked chronic granulomatous disease (fourth update). *Blood Cells Mol. Dis.* **90**, 102587 (2021).
59. M. C. Dinauer, Disorders of neutrophil function: An overview. *Methods Mol. Biol.* **412**, 489–504 (2007).
60. I. Sarfraz *et al.*, 6-Phosphogluconate dehydrogenase fuels multiple aspects of cancer cells: From cancer initiation to metastasis and chemoresistance. *Biofactors* **46**, 550–562 (2020).
61. M. H. Paclet, S. Berthier, L. Kuhn, J. Garin, F. Morel, Regulation of phagocyte NADPH oxidase activity: Identification of two cytochrome b558 activation states. *FASEB J.* **21**, 1244–1255 (2007).
62. W. Fischle *et al.*, Enzymatic activity associated with class II HDACs is dependent on a multiprotein complex containing HDAC3 and SMRT/N-CoR. *Mol. Cell* **9**, 45–57 (2002).
63. Y.-P. Wang *et al.*, Regulation of G6PD acetylation by SIRT2 and KAT9 modulates NADPH homeostasis and cell survival during oxidative stress. *EMBO J.* **33**, 1304–1320 (2014).
64. C. Shan *et al.*, Lysine acetylation activates 6-phosphogluconate dehydrogenase to promote tumor growth. *Mol. Cell* **55**, 552–565 (2014).
65. F. Meissner, K. Molawi, A. Zychlinsky, Superoxide dismutase 1 regulates caspase-1 and endotoxic shock. *Nat. Immunol.* **9**, 866–872 (2008).
66. A. de Luca *et al.*, IL-1 receptor blockade restores autophagy and reduces inflammation in chronic granulomatous disease in mice and in humans. *Proc. Natl. Acad. Sci. U.S.A.* **111**, 3526–3531 (2014).
67. K. Campbell, J. Vowinckel, M. A. Keller, M. Ralser, Methionine metabolism alters oxidative stress resistance via the pentose phosphate pathway. *Antioxid. Redox Signal.* **24**, 543–547 (2016).
68. J. Ji *et al.*, Methionine attenuates lipopolysaccharide-induced inflammatory responses via DNA methylation in macrophages. *ACS Omega* **4**, 2331–2336 (2019).
69. A. C. Pfalzer *et al.*, S-adenosylmethionine mediates inhibition of inflammatory response and changes in DNA methylation in human macrophages. *Physiol. Genomics* **46**, 617–623 (2014).
70. S. D. Rosenzweig, Inflammatory manifestations in chronic granulomatous disease (CGD). *J. Clin. Immunol.* **28**, 67–72 (2008).
71. C. A. Dinarello, The IL-1 family of cytokines and receptors in rheumatic diseases. *Nat. Rev. Rheumatol.* **15**, 612–632 (2019).
72. R. Lin *et al.*, 6-Phosphogluconate dehydrogenase links oxidative PPP, lipogenesis and tumour growth by inhibiting LKB1-AMPK signalling. *Nat. Cell Biol.* **17**, 1484–1496 (2015).
73. S. Daneshmandi *et al.*, Blockade of 6-phosphogluconate dehydrogenase generates CD8(+) effector T cells with enhanced anti-tumor function. *Cell Rep.* **34**, 108831 (2021).
74. J. L. Guerriero *et al.*, Class IIa HDAC inhibition reduces breast tumours and metastases through anti-tumour macrophages. *Nature* **543**, 428–432 (2017).
75. W. J. Zhang, H. Wei, Y. T. Tien, B. Frei, Genetic ablation of phagocytic NADPH oxidase in mice limits TNFα-induced inflammation in the lungs but not other tissues. *Free Radic. Biol. Med.* **50**, 1517–1525 (2011).
76. X.-P. Gao *et al.*, Role of NADPH oxidase in the mechanism of lung neutrophil sequestration and microvessel injury induced by gram-negative sepsis: Studies in p47phox−/− and gp91phox−/− mice. *J. Immunol.* **168**, 3974–3982 (2002).
77. B. Manoury *et al.*, The absence of reactive oxygen species production protects mice against bleomycin-induced pulmonary fibrosis. *Respir. Res.* **6**, 11 (2005).
78. P. A. Barry-Lane *et al.*, p47phox is required for atherosclerotic lesion progression in ApoE(-/-) mice. *J.Clin. Invest.* **108**, 1513–1522 (2001).
79. W. J. van Zuylen *et al.*, Macrophage activation and differentiation signals regulate schlafen-4 gene expression: Evidence for Schlafen-4 as a modulator of myelopoiesis. *PLoS One* **6**, e15723 (2011).
80. S. Chang *et al.*, Histone deacetylase 7 maintains vascular integrity by repressing matrix metalloproteinase 10. *Cell* **126**, 321–334 (2006).
81. K. Hoshino *et al.*, Cutting edge: Toll-like receptor 4 (TLR4)-deficient mice are hyporesponsive to lipopolysaccharide: Evidence for TLR4 as the Lps gene product. *J. Immunol.* **162**, 3749–3752 (1999).